CL-TWE Mach–Zehnder electro-optic modulator based on InP-MQW optical waveguides

Guang Qian (钱 广)[1,*,†], Bin Niu (牛 斌)[1,†], Wu Zhao (赵 武)[2], Qiang Kan (阚 强)[2], Xiaowen Gu (顾晓文)[1], Fengjie Zhou (周奉杰)[1], Yuechan Kong (孔月婵)[1], and Tangsheng Chen (陈堂胜)[1]

[1]*Science and Technology on Monolithic Integrated Circuits and Modules Laboratory, Nanjing Electronic Devices Institute, Nanjing 210016, China*

[2]*Key Laboratory of Semiconductor Materials Science, Institute of Semiconductors, Chinese Academy of Sciences, Beijing 100083, China*

**Corresponding author: chinaqgll@163.com*

Received November 26, 2018; accepted March 8, 2019; posted online May 29, 2019

In this Letter, we reported the preliminary results of an integrating periodically capacitive-loaded traveling wave electrode (CL-TWE) Mach–Zehnder modulator (MZM) based on InP-based multiple quantum well (MQW) optical waveguides. The device configuration mainly includes an optical Mach–Zehnder interferometer, a direct current electrode, two phase electrodes, and a CL-TWE consisting of a U electrode and an I electrode. The modulator was fabricated on a 3 in. InP epitaxial wafer by standard photolithography, inductively coupled plasma dry etching, wet etching, electroplating, etc. Measurement results show that the MZM exhibits a 3 dB electro-optic bandwidth of about 31 GHz, a V_π of 3 V, and an extinction ratio of about 20 dB.

OCIS codes: 130.3120, 250.4110, 230.4205.
doi: 10.3788/COL201917.061301.

A large-bandwidth and low half-wavelength-voltage (V_π) Mach–Zehnder electro-optic (EO) modulator is an urgent need for the fields of high-speed optical communication and microwave photonics[1–4]. At present, the main materials for an EO modulator include $LiNbO_3$[5], III–V semiconductor materials[6,7], silicon[8,9], and polymer[10]. Especially, the EO modulator made of InP-based multiple quantum well (MQW) optical waveguides with capacitive-loaded (CL) traveling wave electrodes (TWEs) has attracted much more attention because of its remarkable advantages. Firstly, the strong index changes induced by the quantum confined Stark effect (QCSE) in the InP-MQW optical waveguides can achieve high EO modulation efficiency and low driving voltage[11]. This is very important for practical application, because the lower the driving voltage is, the lower the consumption, cost, and size of the modulator become. The length of this type of modulator is only several millimeters. More importantly, this type of EO modulator can be potentially integrated with a wide range of InP-based components such as lasers, semiconductor optical amplifiers (SOAs), photodetectors (PDs), passive optical circuits, and even electronic drivers[2,12,13]. This is very attractive for achievement of the complex and multifunctional optoelectronic integrated chips.

In this Letter, we present the performance results of a CL-TWE Mach–Zehnder modulator (MZM) based on InP-MQW optical waveguides. The device has a 3 dB EO bandwidth of about 31 GHz, a V_π of 3 V, and an extinction ratio (ER) of about 20 dB. It has promising applications in optical communication and microwave photonics.

Figure 1(a) shows structure schematic of the EO modulator based on InP-MQW optical waveguides. The device is composed of a Mach–Zehnder interferometer (MZI) based on InP-MQW optical waveguides, a direct current (DC) bias pad, two phase electrodes, a 50 Ω thin-film resistor, and a CL-TWE consisting of a U electrode and an I electrode. The U electrode and I electrode are, respectively, used as the signal electrode (S) and the ground electrode (G). The RF signal was applied to the device from the same side of the two electrodes. On the other side,

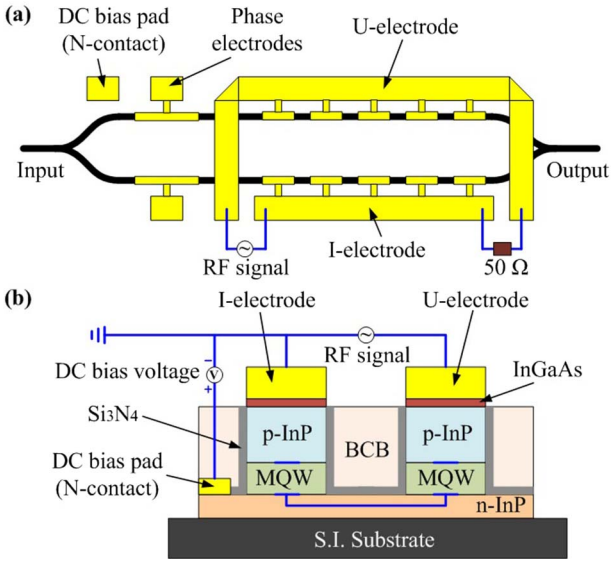

Fig. 1. Schematic diagram of the CL-TWE MZM based on InP-MQW optical waveguides.

a 50 Ω thin-film resistor was fabricated to connect the U electrode and I electrode. The light is input into the optical MZI from one port of the device and modulated by the RF signal in the active region through the CL-TWE. The modulated light is output from the other port of the MZI. The DC pad is used to provide bias voltage for the modulator. Phase shifts in the two arms can be realized by the corresponding phase electrodes. In this device, the MZI is working at the push–pull configuration, as shown in Fig. 1(b). The RF signal loaded on the U and I electrodes floats through the negative (n) InP between the two MQW capacitors. The DC bias voltage is applied via the DC pad, which is several hundreds of micrometers away from the RF relevant capacitors. The U and I electrodes connect with the corresponding MQW layers through the positive (p) InP layer. The output intensity transfer function of the MZI can be written in the form of $T_{\mathrm{MZI}} = \cos^2(\Delta\varphi/2)$, where $\Delta\varphi$ is the phase difference between the two arms of the MZI[14]. Therefore, the phase difference between the two arms directly determines the output optical intensity of the MZI. The phase of light in the arm can be changed by the applied voltage on the corresponding electrode based on the EO property of the InP-MQW layer.

Figure 1(b) shows the cross sectional sketch of the MZM based on InP-MQW optical waveguides. The waveguide in the modulator contains an InGaAs ohmic contact layer, p-InP upper cladding layer, InGaAsP MQW core layer, n-InP lower cladding layer, and semi-insulating InP substrate. The DC bias pad contacts with the n-InP layer and is positioned outside of the interferometer on the MZI mesa. The phase electrodes and the inner segmented electrodes of the U and I electrodes contact with the surface InGaAs layer. The deep InP-MQW optical waveguides are passivated by the Si_3N_4 layer and embedded in benzocyclobutene (BCB) polymer. The Si_3N_4 layer in the device mainly plays a role of etching stop layer for the BCB dry etching process. The thickness of the Si_3N_4 layer is much smaller than that of the InP-MQW optical waveguide. In addition, the large refractive index difference between the Si_3N_4 and the InP-MQW waveguide ensures that the optical field is mainly confined in the InP-MQW waveguide layer. Therefore, the effect of the thin Si_3N_4 layer on the processing of the optical signal is very small and can be neglected. The coated BCB was used for InP-MQW waveguide over-cladding and planarization. The TWE can be fabricated on the surface of the BCB layer with equal height to avoid climbing. Importantly, the insert low-ε_r BCB layer between the n-InP layer and the TWE can induce the performance improvements. First, the microwave effective refractive index of the TWE can be reduced by the low-ε_r BCB to achieve a better match with the optical index. Consequently, the bandwidth of the modulator can be further improved compared to the modulator without the BCB layer. Secondly, the position of the electric field between the two electrodes after using BCB is higher. The field that is buried in the substrate is correspondingly smaller, so the dielectric loss of the TWE is less than in the case without the BCB layer. In addition, the loading capacitance generally can be calculated by $C_L = (n_{\mathrm{opt}}^2 - n_\mu^2)/(c \cdot Z_m \cdot n_{\mathrm{opt}})$, where, n_{opt}, n_μ, Z_m, and c, respectively, are the optical grope index, microwave effective refractive index, characteristic impedance, and light speed in free space[14]. Therefore, the capacitive load will be changed after using the BCB layer.

To ensure the single-mode propagation of light in the InP-MQW optical waveguide, the single-mode condition was calculated by using the effective refractive index method. Figure 2 shows the calculated effective refractive indices of InP-MQW optical waveguides for TE_{00} mode and TE_{01} mode with different waveguide widths. It indicates that the InP-MQW optical waveguide supports the single mode in the case of the waveguide width being less than 2.5 μm. Taking into consideration the fabrication difficulty, the 2-μm-wide waveguide was used. The corresponding calculated effective refractive index is about 3.261.

In the CL-TWE MZM, the inner segmented electrodes of the U and I electrodes used to modulate the optical wave are equally divided into many small sections. Each of the sections is connected to the outer electrodes periodically, as shown in Fig. 1(a). In this device, the modulation sections are arranged periodically with the period length of 250 μm along the two arms of the MZI and are connected with the outer electrodes via the surface of the BCB layer. The length of the effective modulation electrodes positioned on the MQW waveguide to provide the EO interaction is 100 μm. Therefore, the fill factor is 0.4, which is an important parameter for tuning the capacitive load.

Figure 3 shows the fabrication processes of the EO modulator based on InP-MQW optical waveguides. The fabrication starts with deposition of a 500-nm-thick SiO_2 layer by plasma-enhanced chemical vapor deposition (PECVD). Then, a hard SiO_2 mask for the dry etching of the MZI optical waveguides with a width of 2 μm was made by using lithography with 0.5 μm precision and dry etching in CHF_3 gas. Under the protection of a

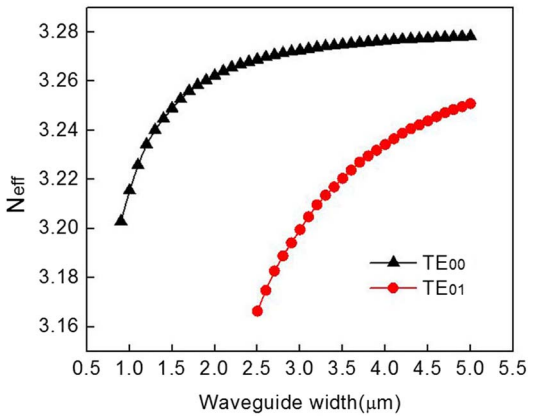

Fig. 2. Calculated effective refractive index of the InP-MQW optical waveguide for TE_{00} mode and TE_{01} mode with different waveguide widths.

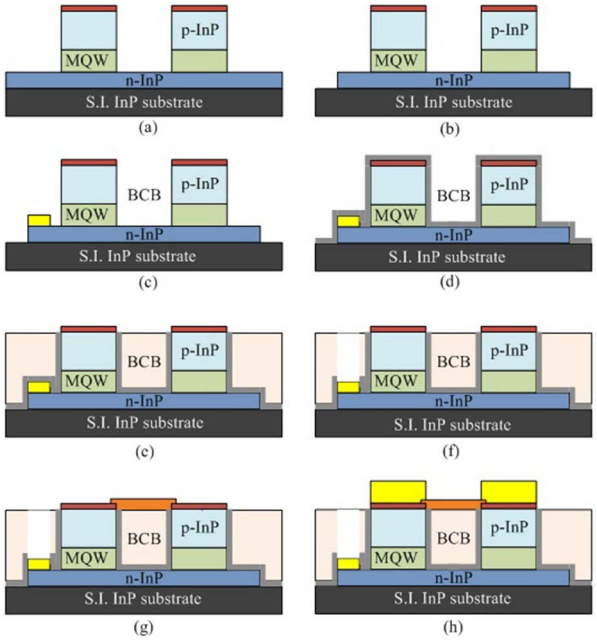

Fig. 3. Schematic process flow of the fabrication of CL-TWE EO MZM based on InP-MQW optical waveguides.

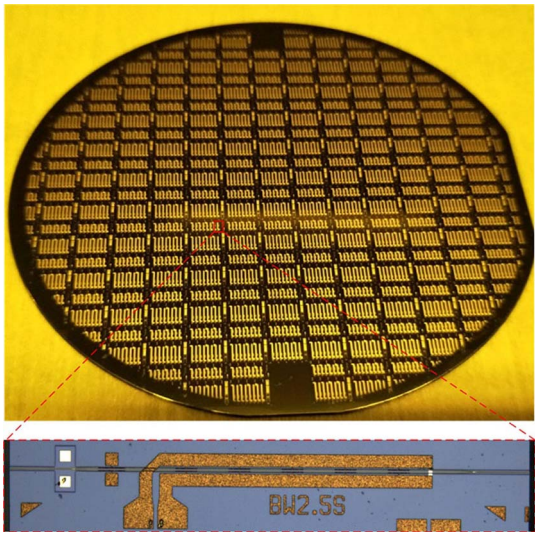

Fig. 4. Photographs of the fabricated 3 in. CL-TWE MZM chip and a single MZM chip based on InP-MQW optical waveguides.

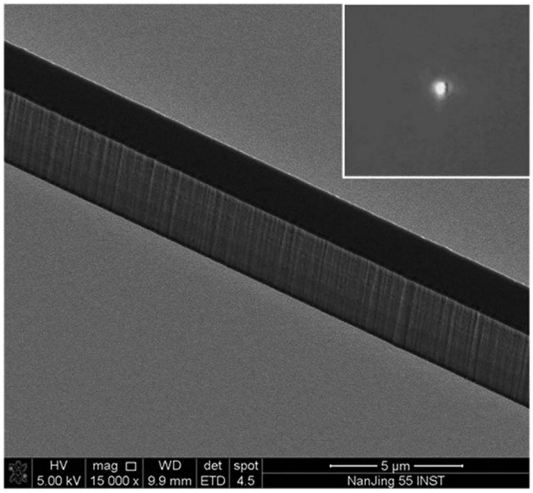

Fig. 5. 45° SEM view of an InP-MQW optical waveguide etched to the n-InP layer without the following processes. Inset: the measured light spot of the InP-MQW optical waveguide.

SiO_2 mask, the InP-MQW waveguide was fabricated by dry etching in a mixed gas of Cl_2 and N_2. The waveguides were etched to the n-InP layer, as shown in Fig. 3(a). Then, the n-InP mesa was wet etched in H_3PO_4:HCl (4:1), as shown in Fig. 3(b). Following this, the N-contacted DC electrode consisting of Ti/Pt/Au was made by using thermal evaporation and lift-off techniques. To ensure the isolation, the Si_3N_4 passivation with a thickness of about 200 nm was performed on the InP-MQW optical waveguides. After this, the planarization process was performed by using BCB polymer. The BCB and Si_3N_4 layers were dry etched to expose the InGaAs layer. Following, a SiO_2 mask was then patterned to open up windows for the N-contacted DC. The BCB polymer layer and the Si_3N_4 layer were successively etched to expose the N-contacted DC electrode. Then, the 50 Ω resistor was formed by magnetron sputtering and lift-off techniques. Finally, the phase electrodes and the CL-TWE consisting of U and I electrodes were fabricated by Au electroplating.

Figure 4(a) shows a photograph of a fabricated 3 in. CL-TWE MZM chip based on InP-MQW optical waveguides. Figure 4(b) shows a single MZM chip with five modulation sections. The total length of the single MZM chip is only about 2 mm. Figure 5 gives the 45° scanning electron microscope (SEM) view of an InP-MQW optical waveguide etched to the n-InP layer without the following processes. The waveguide exhibits a smooth side wall.

In order to show the performance of the fabricated MZM, we firstly measured the optical characteristics of the InP-MQW optical waveguides in the EO modulator. By using the Fabry–Perot cavity interference fringe contrast ration method, we obtained that the optical waveguide has a propagation loss of about 0.94 dB/mm. For the 2-mm-long InP-MQW optical waveguide, it has an entire insertion loss of about 20 dB, including the propagation loss and the coupling loss between coupling fiber and InP waveguide at the input and output ports. According to the propagation loss of the waveguide, the on-chip loss is only about 2 dB. Therefore, the coupling loss is about 9 dB per facet and is the main contributor of insertion loss. This is mainly because of the optical mode mismatch between the fiber and the InP-MQW optical waveguide. In order to reduce the coupling loss to satisfy the low-loss requirement of the optical system, both the optical lens and the spot size converter (SSC) are effective methods to be used.

In addition, the EO characterizations of the MZM were also measured. In the measurement, a wavelength tunable laser, polarization controller, erbium-doped fiber amplifier (EDFA), PD, vector network analyzer, and DC voltage

source were utilized. The wavelength tunable laser was used as laser source. The polarization controller was used to control the polarization state of the input light into the MZM. The PD and the vector network analyzer were used to monitor the output power and to measure the S parameters, respectively. The DC source was used to provide bias voltage for the device. In order to ensure the measurement accuracy, short-open-load-through (SOLT) calibration was firstly performed before the response test.

First, we measured the DC characteristic at an operating wavelength of 1557 nm. The output optical power from the MZM with differential bias voltage applied on a single arm was monitored by an optical power meter, as shown in Fig. 6. It indicates that the ER of the MZM reaches up to about 20 dB. The device exhibits a V_π of about 3 V that is lower than that of the traditional $LiNbO_3$ MZM. In this device, the photoluminescence peak wavelength of the MQW layer is designed at about 1430 nm. This is far away from the operation wavelength of 1557 nm and leads to low optical absorption. Therefore, the electric-field-induced index change is sufficiently large for efficient phase modulation and is the main reason contributing to the extinction in Fig. 6. We also measured the EO response of the modulator based on InP-MQW optical waveguides at 1557 nm. The measurement of EO response was performed using an RF power of about 0 dBm and a DC bias of about −4.3 V at the operation point. The device shows a 3 dB EO bandwidth of larger than about 30 GHz, as shown in Fig. 7.

The performance of this device is wavelength dependent of the input optical signal. First, the bandwidth of the modulator is mainly determined by the velocity mismatch factor $\beta_{\text{opt}}^{\mu} = \omega_m(n_\mu - n_{\text{opt}})/c$, where ω_m, n_μ, n_{opt}, and c, respectively, are the modulation frequency, optical grope index, microwave effective refractive index, and light speed in free space[15], in which n_{opt} is wavelength dependent. Secondly, the phase and absorption in the MQW optical waveguide are also wavelength dependent.

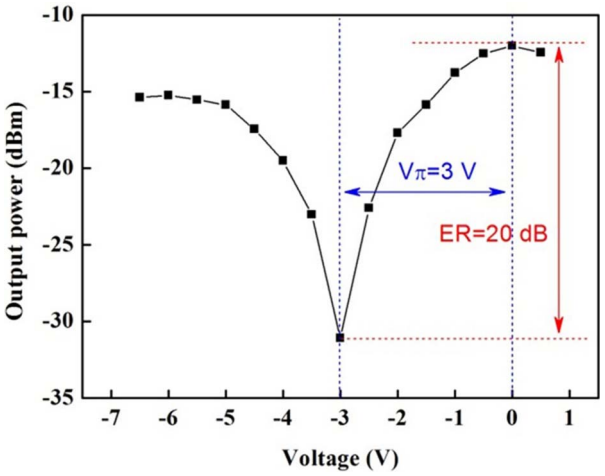

Fig. 6. Measured V_π and ER characteristics of the InP-MQW EO MZM.

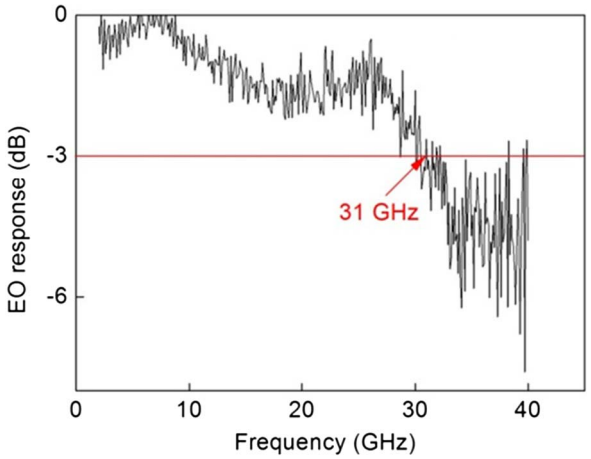

Fig. 7. EO response of the InP-MQW EO MZM.

Therefore, both the RF small signal characteristics and DC characteristics are all wavelength dependent.

In summary, we reported our work on CL-TWE EO MZM based on InP-MQW optical waveguides. The single-mode condition of the InP-MQW optical waveguide was calculated by using the effective refractive index method. By using standard techniques of photolithography, dry etching, wet etching, magnetron sputtering, lift off, and electroplating, the MZM chip was fabricated on a 3 in. InP epitaxial wafer. To characterize the performance of the EO modulator, the optical propagation loss, light spot, DC ER characteristic, and EO response were measured, respectively. The fabricated device with five modulation periods has a length of about 2 mm. Experimental results show that the InP-MQW optical waveguide has a propagation loss of about 0.94 dB/mm. The modulator exhibits a 3 dB EO bandwidth of about 31 GHz, a V_π of about 3 V, and an ER of about 20 dB. The CL-TWE EO MZM has the remarkable advantage of small size and huge potential for larger bandwidth and lower V_π. It will be widely used in high-speed optical communication, microwave photonics, etc.

†These authors contributed equally to this work.

References

1. K. Liu, C. R. Ye, S. Khan, and V. J. Sorger, Laser Photon. Rev. **9**, 172 (2015).
2. S. Lange, M. Gruner, C. Meuer, R. Kaiser, M. Hamacher, K. Velthaus, and M. Schell, J. Lightwave Technol. **34**, 401 (2016).
3. J. Capmany and D. Novak, Nat. Photon. **1**, 319 (2007).
4. Y. Wang, K. Wu, and J. Chen, Chin. Opt. Lett. **16**, 020003 (2018).
5. P. O. Weigel, J. Zhao, K. Fang, H. Alrubaye, D. Trotter, D. Hood, J. Mudrick, C. Dallo, A. Pomerene, A. Starbuck, C. DeRose, A. Lentine, G. Rebeiz, and S. Mookherjea, Opt. Express **26**, 23728 (2018).
6. Y. Ogiso, J. Ozaki, Y. Ueda, N. Kashio, N. Kikuchi, E. Yamada, H. Tanobe, S. Kanazawa, H. Yamazaki, Y. Ohiso, T. Fujii, and M. Kohtoku, J. Lightwave Technol. **35**, 1450 (2017).
7. Y. Xiang and S. Pan, Front. Optoelectron. **9**, 497 (2016).
8. M. Li, L. Wang, X. Li, X. Xiao, and S. Xu, Photon. Res. **6**, 109 (2018).
9. Q. Xu, S. Bradley, P. Sameer, and L. Michal, Nature **435**, 325 (2005).

10. J. Tang, L. D. Wang, R. Z. Li, Q. Zhang, and T. Zhang, Modern Phys. Lett. B **30**, 7902607 (2016).
11. S. Dogru and N. Dagli, Opt. Lett. **39**, 6074 (2014).
12. L. Augustin, S. Rui, E. D. Haan, S. Kleijn, P. Thijs, S. Latkowski, D. Zhao, W. Yao, J. Bolk, S. Mingaleev, A. Richter, A. Bakker, and T. Korthorst, IEEE J. Sel. Top. Quant. Electron. **24**, 6100210 (2017).
13. L. Zhang, in *Proceedings of Asia Communications & Photonics Conference & Exhibition* (2009), paper WD1.
14. H. Chen, "Development of an 80 Gbit/s InP-based Mach–Zehnder Modulator" Ph.D. dissertation (Berlin Technical University, 2007).
15. M. U. Sadiq, B. Roycroft, J. O'Callaghan, P. Morrissey, W. Han, F. H. Peters, and B. Corbett, in *Proceedings of Irish Signals & Systems Conference & China-Ireland International Conference on Information & Communications Technologies*, IET (2014), p. 123.